The Role of Impedance Matching for Depth Adjustment of Inductive Charger for Medical Implants

Oleg Gorskii

Saint Petersburg State University of Aerospace Instrumentation (SUAI), Saint Petersburg State University (SPbU)
Saint Petersburg, Russian Federation
gorskijoleg@gmail.com

***Abstract*—The paper describes the power supply method of implantable devices using inductive wireless power transfer for the built-in battery charge. Spiral transmitting PCB inductor 100x100 mm and toroidal receiving PCB inductor 30x20 mm are used. The charging current distribution at various relative positions of the transmitting and receiving inductors is explored. Analytically calculated values are compared to the bench test results in the air and imitation environments. The maximum charging current was achieved in the receiving inductor location area, which is determined by the equipotential value zone of the inductor coupling coefficient, which ensures the load matching in a system. With a coaxial arrangement of the inductors, the maximum was reached at a distance of 35 mm between them.**

I. Introduction

We can distinguish three most common areas of implantable devices placement: subcutaneous, intramuscular and intraperitoneal. Introduction simplicity and withdrawal of the device, minimal traumatic operation as well as an increased damage risk or displacement of the device, its electrodes and negative cosmetic effect characterize the subcutaneous method. Opposing properties have methods of intramuscular and intraperitoneal implantation, which makes them more preferable to use, including the potential increase in implant lifetime with a wireless power transmission module. The priority range of energy transfer considered to be the depth of the muscle layer of the human or abdominal cavity of a small laboratory animal, i.e. the range is 20 ... 50 mm.

When considering the methods of wireless power transfer (WPT), the range and efficiency problems come to the fore. The efficiency of the WPT system is important from two points of view. Firstly, the higher the efficiency, the less energy is absorbed by the tissues. Secondly, when implementing WPT powered by an external portable battery, its discharge rate and, as a result, the ergonomics of the entire system as a whole depend on the transfer efficiency. According to scientific literature sources, the greatest transfer efficiency at the actual depth of implantation was achieved in works based on inductive and ultrasound methods [1].

This research purpose is to estimate the battery charging current's achievable levels and their distribution, depending on the relative position of the coils using the practical implementation of the inductive WPT system.

II. Experimental setup

A. Schematics

The resonance effect was used in the overwhelming majority of the WPT system implementations described in the scientific literature. This makes it possible to minimize the reactive part of the inductor resistance and substantially increase the transfer efficiency in the ferro- and ferrimagnetic core absence. The system of inductors, in the simplest case, consists of two resonant circuits [2-5]. A series resonance circuit is usually used on the generator side in view of the small output amplifier resistance, while on the receiving side the choice is ambiguous [6]. For high-resistance loads (RFID, etc.), the use of parallel circuits is more efficient and vice versa.

The transfer efficiency depends significantly on the distance between the coils and for systems with two inductors it usually does not exceed 60% at a distance of several tens millimeters in the laboratory conditions. This is due to a decrease of the mutual inductance between the inductors as they distance from each other and the reduced quality factor Q of the resonance circuits caused by connection of the amplifier and the payload circuits. The idea of placing intermediate galvanically isolated high-Q resonance circuits between the primary and output coils, which allows increasing efficiency, goes back to the time of Nikola Tesla. In modern studies focused on implants, this idea is reflected in the use of an additional one [7-8] or two inductors [9-11]. In case of 3-inductor system, the additional inductor placement on the generator side can potentially improve the WPT's efficiency without increasing the implant size and changing its layout, while its introduction in addition to the receiving inductor reduces the negative effect of the low-Q output circuit. In [7] was demonstrated more than 50% increase of efficiency while using two resonant circuits in one plane on the transmitting side and at a distance of WPT of 12 mm. In work [8], an additional resonant circuit on the receiving side allows to increase the efficiency of around 10 % at a distance of 15 mm. The use of 4-inductor system can potentially be the most effective solution. In the article [11] it was demonstrated that at a distance of 5 mm there is practically no difference in effectiveness between 2 and 4-inductor systems, whereas at a 10 ... 50 mm distance at least a double advantage of 4-inductor system was displayed. Nevertheless, for each individual configuration, this hypothesis should have

ISSN 2305-7254

an analytical confirmation, since there is an opinion that there is no increase in efficiency from the additional inductors installation under certain conditions [12]. In any case, the more resonant circuits will be introduced into the system, the more difficult it will be to adjust them to a single resonant frequency and save it in a practical implementation.

In view of the foregoing, a system with two series resonant circuits was chosen. Inductors' parameters and characteristics will be considered in the next subsection.

The main types of amplifiers used for this task are high-efficiency class E [3], [5], [11], [13-18] and class D [19-23], which are devices operating in a key mode. The efficiency of such amplifiers can reach up to 90 % with minimum set of components and a low heat dissipation.

In view of the simplicity in implementing the output power and the operating frequency adjustment by the pulse-width modulation (PWM), a D class amplifier on transistors IRF6708S2 was chosen. PWM duty cycle for this type of amplifier varies in range 10...50 %. The output power herewith is nonlinearly dependent on the PWM duty cycle, which usually requires feedback. The generator operated at a frequency of 879.5 kHz. The supply voltage was 23.6 V. The current amplitude in the transmitting resonant circuit in the idle mode was 930 mA. The transmitting circuit resonant frequency was 878.5 kHz. The resonance frequency of the receiving circuit was 876 kHz. Resonant capacitors were chosen with an NP0 dielectric having the best thermal stability.

The printed circuit boards (PCB) of the receiving module, in addition to the inductor, contained seats for a resonant capacitor, a protective Zener diode (BZV55-6V8), a full-bridge diode rectifier (BAT54), and a filter capacitor. The Zener diode is effective for protecting the receiving module's integrated circuits from short-term voltage pulses that do not lead to its significant heating. Standard diode circuits can be used as rectifiers: a quarter bridge, a half bridge and a full bridge [5], [15-17], [21], [24]. Diodes can be partially or completely replaced by transistors directly commutated by the input signal [3], [24], [25]. Also complementary metal-oxide-semiconductor (CMOS) circuits can be used, functionally realized either by the principle of "active diodes" [26], [27], or actively controlled transistors [28], [29]. The choice of the rectifier circuit is essential in the WPT system as a part of implantable device because it can be one of the heating sources of the receiving module. Nevertheless, in this paper the simplest variant for implementation was chosen.

Polymer encapsulation was used for sealing the receiving module. The integrated charge control circuit (MC34671) and a Li-ion 2000 mAh battery were located outside the receiving module. The voltage on the battery was maintained at 3.8 V between the measurements series, and the voltage variation effect during the series was neglected due to the significant difference between the battery capacity and the charge transferred to it. As the target level of the charging current, the 100 mA value was chosen, which would allow to charge small medical grade batteries like Quallion QL0200I-A in a few hours.

B. Inductors

Inductors can be made of either single-core wire [5, 10, 30], or of a litz wire, which reduces the coil frequency-dependent active resistance by increasing the cross-sectional area of the surface conductive layer [9, 15, 17]. It should be noted that the frequency determines the cores number in the litz wire: 15...800 kHz at 10 cores, 15...1000 kHz at 20 cores, 15...1700 kHz at 60 cores [31], which can limit its use as the required coils dimensions decrease. Also, inductors are manufactured on a printed circuit board with a hard [5], [8], [14], [32] or flexible base [33], on a glass substrate [34], in the flowing metal form conductor injected into the channel on a flexible silicone base [35] and so on. In all cases, except the last, the conductor has a rectangular cross-section.

One of the main limitations for inductors is their permissible overall dimensions [36], determined by the ergonomic implant dimensions. The achievable inductance in a given volume, determined by the allowable windings placement density in the section of the coil, depends on the coils manufacturing technology. On the other hand, the parasitic resistance depends on the material resistance, the cross-sectional conductor area, on the turn's density and location configuration due to the proximity effect, and also on the shape and cross-sectional area due to the skin effect, which together is also determined by the used technology. Finally, the parasitic capacitance also depends on the parameters listed above, as well as on the dielectric constant of the insulator. Each of these technologies allows you to vary the listed parameters in a fairly wide range, so whatever technology method has been chosen, each of them will have to solve the optimization problem of choosing acceptable coil parameters.

In the present work, inductors were made on single- and multilayer PCB based on FR-4 laminate (Fig. 1). This type of coils was chosen due to the fact that this method allows promptly receive prototypes of different inductors configurations for research. Each new configuration of the wound coil needs a production of new template for its winding, while the PCB inductors made it possible to obtain a relatively high reproduction level of the conductor's geometry and significant "freedom" in the choice of shapes and turns distribution in the coil's cross section.

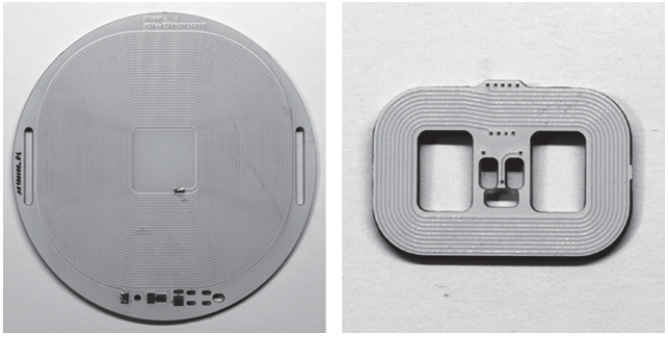

Fig.1. Transmitter (left) and receiver (right) inductors

The inductors have the shape of a rounded rectangle which, when used with a similarly shaped implant, allows to use its internal space in the most efficient way and reaches larger inductance values by increasing the length of the winding. The need for rounded corners can be dictated both by the case shape

and by avoiding the conductor bends at a right angle to reduce the active resistance and to reduce the effect of re-reflection and additional high frequency signals radiation at the parasitic components resonant frequencies. Their characteristics are given in "Table I". Among them: *a* - overall width, *b* - overall depth, *r* – overall spherical radius, *h* - overall winding height, *w* - overall width of winding, *N* - number of turns (layers number and turns in them), *H* - the conductor's height, *W* - the conductor's width, *G* - gap between the conductors, *l* - the conductor's length.

TABLE I. GEOMETRY PARAMETERS OF PCB INDUCTORS

Parameter	Transmitter coil	Receiver coil
a, [mm]	100,45	29
b, [mm]	99,4	19
r, [mm]	40,25	5,75
h, [mm]	0,105	1,1
w, [mm]	37,4	4,25
N	1×36	5×9
H, [µm]	105	35
W, [µm]	700	250
G, [µm]	350	250
l, [m]	7,74	3,321

The PCB inductor's turns were actually located with some displacement relatively to the conventional rectangular grid (Fig. 2), the conductor's density and width also varied. Hereby, the variability of the dielectric layer's thickness was determined in part by the PCB manufacturing technology. These factors knowingly made an error in estimating the geometric parameters values of both inductors listed in "Table I".

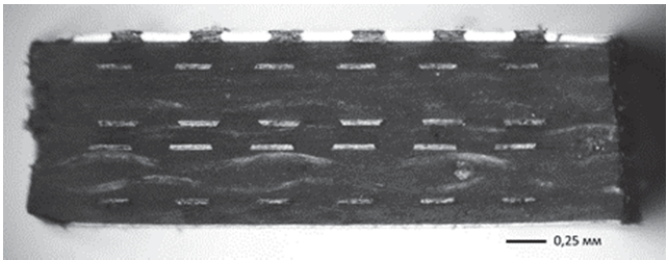

Fig.2. The receiver coil cross section with 5×6 turns for example

The inductor parameters were evaluated using an impedance analyzer WK6510B using a four-wire scheme with averaging over 10 measurement cycles (Fig. 3). Taking into account the equivalent inductor circuit (Fig. 4), the measured impedance *Z* was expressed in terms of the inductance values *L* and the parasitic resistance R_p and the capacitance C_p:

$$Z(\omega) = (j\omega L + R_p)||\,(1/j\omega C_p). \quad (1)$$

It was further assumed that only the component R_p is essentially dependent on the frequency, in view of the skin effect and the proximity effect, in contrast to *L* and C_p. This assumption was made in view of the fact that during the measurements, the inductor was suspended in the air at least 200 mm distance from the conducting and magneto-active materials, and the dielectric permittivity of the used insulating materials in the considered frequency range changed insignificantly.

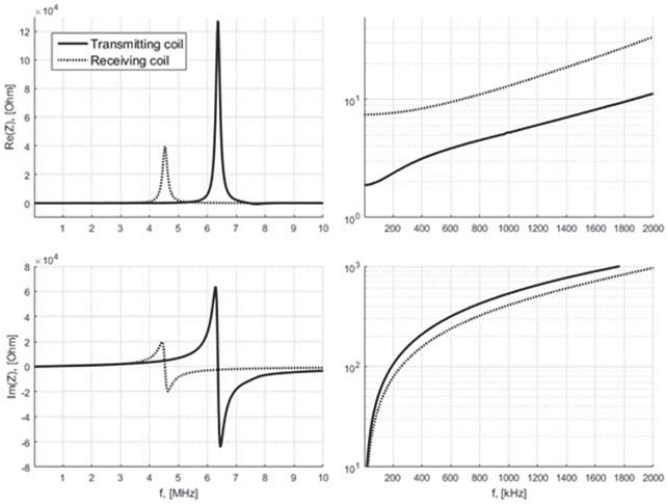

Fig.3. Measured inductor's impedances

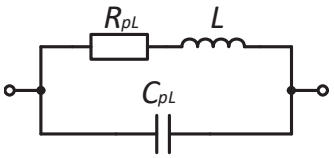

Fig.4. Inductor equivalent circuit

From (1), the active impedance part:

$$Z_{Re}(\omega) = \frac{R_p(\omega)}{\left(1 - \omega^2 L C_p\right)^2 + \omega^2 C_p^2 R_p^2(\omega)}. \quad (2)$$

Imaginary part of the impedance:

$$Z_{Im}(\omega) = \frac{\omega L - \omega^3 L^2 C_p - \omega C_p R_p^2(\omega)}{\left(1 - \omega^2 L C_p\right)^2 + \omega^2 C_p^2 R_p^2(\omega)}. \quad (3)$$

At low frequencies, the capacitive component has practically no effect on the imaginary impedance part (the self-resonance frequency of the coils exceeds several megahertz), so obtained at 1 kHz value was interpreted as a purely inductive component. Consequently, the self-inductance was calculated as:

$$L \cong \left.\frac{Z_{Im}(\omega)}{\omega}\right|_{\omega=2\cdot\pi\cdot1000} \quad (4)$$

The self-resonance frequency f_{sr}, of the coils after equating to zero numerator of the impedance imaginary part (3), is expressed as:

$$f_{sr} = \frac{1}{2\pi}\sqrt{\frac{1 - R_p^2\, C_p/L}{L C_p}}. \quad (5)$$

For $R_p^2\, C_p/L \ll 1$, when typical R_p values are within tens Ohms, C_p – is tens pF, and L – is tens of μH, the self-resonant frequency can usually be expressed by Thompson's formula precisely to a kilohertz, which implies that the parasitic capacitance could be approximately calculated as:

$$C_p \cong \frac{1}{(2\pi f_{sr})^2}\frac{1}{L} \tag{6}$$

The inductor's active direct-current resistance $R_{p\,DC}$ was determined from the initial value of the impedance real part measured characteristic. In turn, the inductor's frequency dependent active resistance $R_{p\,AC}$ at the generator frequency of 880 kHz was derived from (2):

$$R_{pAC}(\omega) = \frac{1 - \sqrt{1 - 4(\omega C_p - \omega^3 L C_p^2)^2 \cdot Z_{Re}^2(\omega)}}{2\omega^2 C_p^2 \cdot Z_{Re}(\omega)} \tag{7}$$

The inductive parameters estimation results are given in "Table II".

TABLE II. MEASURED CHARACTERISTICS OF PCB INDUCTORS

Parameter	Transmitter coil	Receiver coil
f_{SR}, [MHz]	6,36	4,53
L, [μH]	83,88	62,34
C_p, [pF]	7,46	19,83
R_{pDC}, [Ω]	1,89	7,5
R_{pAC},880 kHz, [Ω]	4,61	10,89

C. *Measurements in air and solution environments*

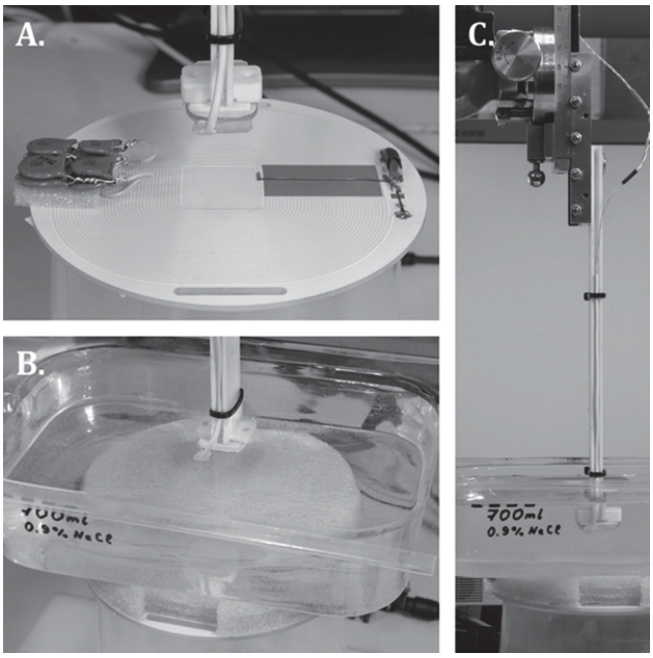

Fig.5. The view of the experimental setup: transmitting and receiving coils in the air environment (A), installation of a container with normal saline on the transmitting coil (B), fixing the sealed receiver module to the manipulator (C)

The experimental setup for carrying out measurements in various environments is presented in Fig. 5. To obtain the charging current value dependence on the position coordinate of the inductor's receiving module, a two-axis manipulator with a stroke of 60 mm along each axes and a 0.1 mm resolution of the measuring scale was used. The transmitting coil was mounted on a plastic base, while in the radius of 150 mm there were no metal or other magneto-active materials. A plastic container with a normal saline (0.9 % NaCl) with dimensions 170×115×45 mm was used as the imitation environment of the biological tissues. The distance from the transmitting inductor to the liquid was 14 mm. The electrical conductivity of the normal soline and blood is close (about 1 S/m), which allows simulating the worst conditions for the electromagnetic field source, because blood has one of the largest electrical conductivity values in the body.

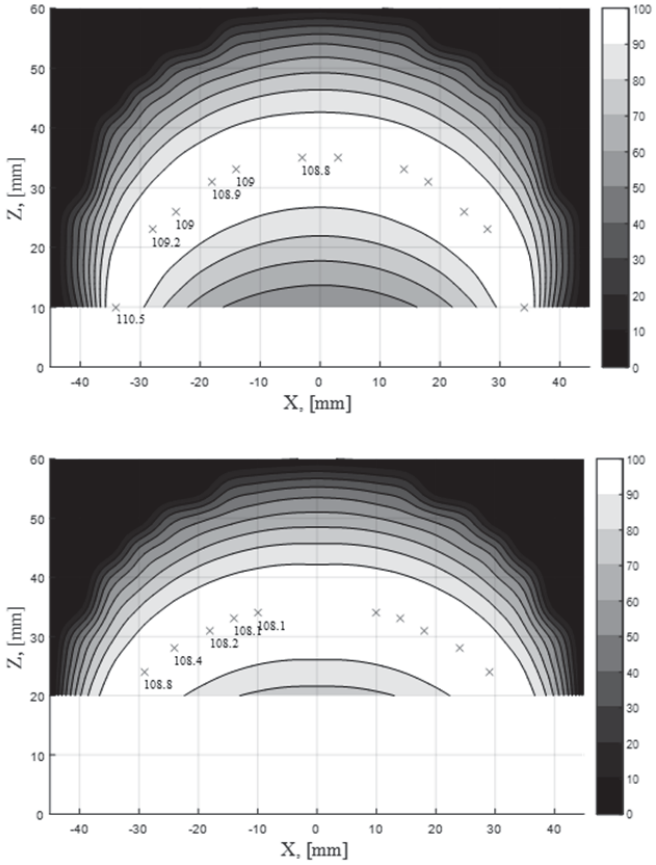

Fig 6. Measured distribution of charging currents in the air (from above) and in the normal saline (from below). The x marks are the points of local maxima.

The charge current distribution was measured by moving the receiving module in the X-Z plane. The origin of the coordinates was in the middle of the transmitting inductor, the Z axis was perpendicular to the coils plane, and the X axis was directed in a parallel way to the receiving inductor's larger side. Based on the assumption that the distribution pattern is symmetric to the Z axis, values were recorded only along the positive X and Z axes values. On the X axis – up to 45 mm in 5 mm steps, along the Z axis – up to 60 mm in 5 mm steps. In

the air environment along the Z axis the measurements were made starting from 10 mm, in a physiological solution starting from 20 mm.

A change in the position of the receiving module led to a change of the reflected impedance on the amplifier side, which affected the current in the transmitting resonant circuit. This was accompanied by heating (within 10 °C) of the resonant capacitor and transmitting coil, which in turn affected the frequency characteristics of the resonant circuit. To minimize this effect, measurements were made in a short time series, alternated with pauses for cooling. The return to the initial state was controlled by the amplitude of the current in the transmitting inductor in idle.

The charge current distributions (Fig.6) showed similarity of results in both environments. This made it possible not to take into account the presence of surrounding biological tissues in subsequent calculations. At the same time, the presence of an equipotential level of charge current maxima can be explained by the effect of load matching in the system. It also demonstrates clearly the relationship of the load matching effect with a most effective depth of implant placement in the tissues.

III. Charging current distribution calculation

For the analytical calculation of the charging current distribution it was first necessary to calculate the inductances of both coils.

Referring to [2], the inductance of one turn, taking into account the winding radius r and the conductor's diameter d and that $d/(2r) \ll 1$, can be calculated by the equation:

$$L(r,d) = \mu_0 r \left(\ln\left(\frac{4r}{d}\right) - 2\right), \tag{8}$$

where $\mu_0 = 4\pi \cdot 10^{-7}$ HN/m is the magnetic constant.

The mutual inductance of two circular turns lying in parallel planes was described in [37] by the equation:

$$M(r_1, r_2, \rho, \delta) = \pi\mu_0\sqrt{r_1 r_2}\int_0^\infty J_1\left(x\sqrt{\frac{r_1}{r_2}}\right) \cdot J_1\left(x\sqrt{\frac{r_2}{r_1}}\right) \cdot J_0\left(x\frac{\rho}{\sqrt{r_1 r_2}}\right) \cdot e^{x\frac{-s}{\sqrt{r_1 r_2}}} dx, \tag{9}$$

where ρ is the axial displacement between the turns, s is the distance between the planes of the turns, J_0 and J_1 are the Bessel functions of the first kind.

The total inductance of the two codirectional inductances is defined as:

$$L = L_1 + L_2 + M_{12} + M_{21} \tag{10}$$

Then, according to the notations assumed in Fig. 7, and using equations (8) - (10) it is possible to express the inductance L_c of the multiturn cylindrical coil:

$$L_c = N_l \sum_{i=1}^{N_w} L_i(r_i, d) + \sum_{n=1}^{N_l}\sum_{m=1}^{N_l}\sum_{i=1}^{N_w}\sum_{j=1}^{N_w} M\left(r_{n,i}, r_{m,j}, 0, s \cdot |n-m|\right) \cdot a_{n,m,i,j}, \tag{11}$$

where N_l is the number of layers, N_w is the number of turns in the layer, $a = 0$ when $n = m$ and $i = j$, $a = 1$ otherwise.

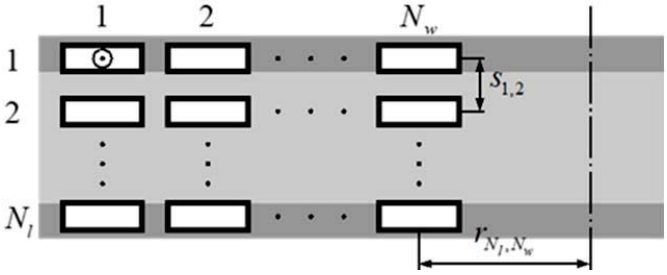

Fig.7. Schematics of turn's placement in cross section of multilayer PCB coil

The inductance of a rectangular coil with rounded corners was also determined by the equation (11) by introducing an equivalent radius parameter r_{eq} of a cylindrical coil. The approximating function for the calculation of r_{eq} was chosen empirically. The boundary values for r_{eq} were determined by radius of equivalent area r_{eqS} and perimeter r_{eqL} of a rectangular coil:

$$r_{eqL} = (r - w/2) + (a + b - 4r)/\pi, \tag{12}$$

$$r_{eqS} = \sqrt{\left((a-w)(b-w) + (\pi-4)(r-w/2)^2\right)/\pi}, \tag{13}$$

where all geometric parameters correspond to those assumed in "Table I".

Using expressions (12-13) the equivalent radius was calculated by:

$$r_{eq} = r_{eqL} - \left(1 - \frac{w}{r_{eqL} + w}\right)\left(r_{eqL} - r_{eqS}\right). \tag{14}$$

Using (11) and (14) calculated inductance values were 83.99 μH (-0.13 %) and 61.79 μH (-0.88 %) for the transmitting and receiving coils, respectively.

The next step was to calculate the values of the inductor coupling coefficient k in the selected range of X-Z values:

$$k = \frac{M}{\sqrt{L_t L_r}}, \tag{15}$$

where M is the mutual inductance of the coils, L_t and L_r are the inductances of the transmitting and receiving coils, respectively.

According to Lyle's method [38], the mutual inductance between two flat coils can be calculated by replacing each of them with two turns whose radii are defined as $r_{avg} \pm w/8\sqrt{3}$, where r_{avg} was replaced by r_{eq} for rectangular inductors with rounded corners. If the transmitting inductor is described by turns A and B, and the receiving inductor by C and D, then their mutual inductance can be described as:

$$M \approx N_t N_r \frac{M_{AC} + M_{AD} + M_{BC} + M_{BD}}{4}, \quad (16)$$

where N_t and N_r are the turns number in one layer of inductors.

After calculating M using equations (9) and (16), as well as inductances of the single layer of each coils (11) and substituting these values in (15), the distribution of k values in the X-Z range was determined (Fig. 9).

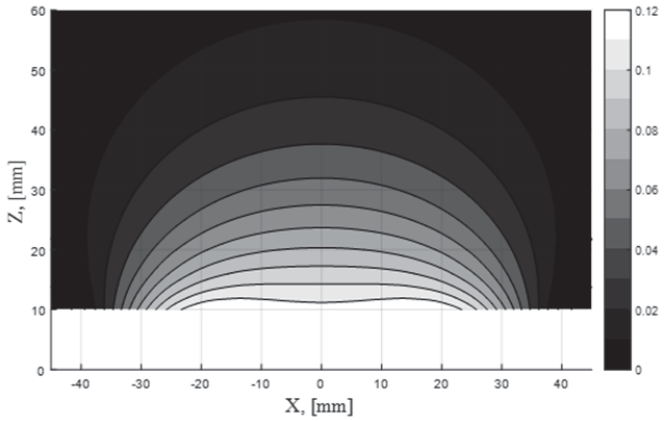

Fig.8. Calculated distribution of coupling coefficient k between transmitting and receiving coils

Calculation of the charging current was carried out by the complex amplitude method. In general, the solution was reduced to a system of equations describing the equivalent scheme of the experimental setup:

$$\begin{cases} E_0 = i_1\left(R_E + R_{Lt} + j\omega L_t + \frac{1}{j\omega C_t}\right) - i_2 \cdot j\omega M \\ i_1 \cdot j\omega M = i_2\left(R_{Lr} + j\omega L_r + \frac{1}{j\omega C_r} + 2R_d + \frac{R_z R_{chg}}{R_z + R_{chg}}\right) \end{cases}, \quad (17)$$

where ω is the operating frequency of the generator, E_0 and R_E are the equivalent voltage and internal resistance of the amplifier, i_1 and i_2 are the currents in the transmitting and receiving resonant circuits, R_{Lt} and R_{Lr} are ohmic resistances of the coils, C_t and C_r are the equivalent resonant capacitor values calculated by $C=1/(\omega_{res}{}^2 L)$, where ω_{res} is the resonant frequency of each circuits in experimental setup, R_d is the resistance of the rectifier bridge diode, R_z is the resistance of the Zener diode, R_{chg} is the resistance of the charge control module with battery.

Calculation of E_0 was based on parameters of the transmitting part during idle state:

$$E_0 = I_0 \sqrt{(R_E + R_{Lt})^2 + \left(\omega L_t - \frac{1}{\omega C_t}\right)^2}, \quad (18)$$

where I_0=930 mA - no-load current in transmitting resonance circuit. The parameter R_E has a nonlinear dependence on the output power and depends on many factors, which made its analytical calculation more difficult. In this regard, it was estimated by bringing the calculated maximum value of the charging current to the maximum value achieved in the experiment and its value was set at 1.6 Ω.

The resistance of the bridge diodes was expressed as:

$$R_d(V) = V \Big/ \left(I_s\left(e^{\frac{q \cdot V}{nkT}} - 1\right)\right), \quad (19)$$

where V is the voltage across the diode, I_s=830·10^{-9} is the reverse saturation current, n=1 – junction constant, k is Boltzmann's constant, T is the temperature in Kelvins, q is the magnitude of an electron charge.

During the experiment, the voltage on the Zener diode did not exceed the threshold voltage for its breakdown, which made it possible to describe its resistance, as:

$$R_z = V_r / I_r, \quad (20)$$

where V_r=4 V – reverse voltage and I_r=2 μA – reverse current.

The permissible value of the charging current was limited by hardware at 150 mA. This value was not reached at any relative position of the coils, which was as an additional protection for the Zener diode from the breakdown. The equivalent resistance of the charge module was expressed as:

$$R_{chg}(V, V_{bat}) = V \Big/ \left(\frac{V - V_{bat}}{R_{ds}} + I_s\right), \quad (21)$$

where V – voltage across charging control IC, V_{bat}=3,8 V – voltage on a rechargeable battery, R_{ds}=0,5 Ω – power MOSFET on resistance, I_s=1,4 mA – IC supply current.

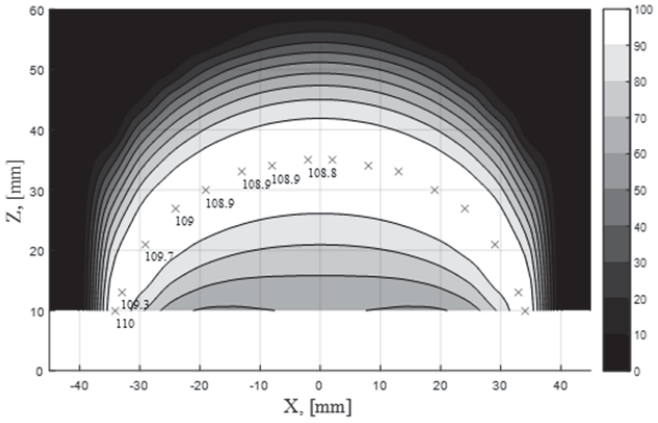

Fig.9. Calculated distribution of charge current [mA]

As a result, the calculated distribution of the charging current corresponded to the experimentally obtained values (Fig. 9). Equipotential levels of charge current values were directly related to the inductor coupling coefficient values, as can be seen from the comparison of Fig. 8 and Fig. 9. At k=0,045, the system was set in the load matching state, which allows us to obtain the maximum value of the charging current.

IV. Conclusion

The WPT system based on two inductively coupled circuits with a series resonance was tested in the air and in the normal saline. The measured values of the current practically did not differ from each other. The indeterminacy of the implant location area in which the charging current was around

100 mA was approximately 0±20 mm along the X axis and 35 ± 5 mm along the Z axis. This area dimensions were determined by the geometry of the coils and the coupling coefficient between them. The proposed analytical description of the system's operation was successfully checked. This will allow to calculate the parameters of inductors under certain requirements regarding the possible location of the implant placement and the level of charging current.

ACKNOWLEDGMENT

The article was prepared in the course of applied research "Development of an experimental sample device for wireless charging of implant batteries" (unique identifier of the project - RFMEFI57817X0233) of the Federal target program "Research and development in priority areas of the scientific and technological complex of Russia for 2014-2020" of the Ministry of Science and Higher Education of the Russian Federation in the priority direction "Life Sciences".

REFERENCES

[1] O. V. Gorskii, "Potential Power Supply Methods for Implanted Devices," *Biomedical Engineering*, 2018, Vol. 52, No. 3, pp. 204-209.

[2] C. M.Zierhofer, E.S.Hochmair, "Geometric Approach for Coupling Enhancement of Magnetically Coupled Coils,"*IEEE Transactions on Biomedical Engineering*, 1996, No 43, pp. 708-714.

[3] P. Cong et al., "A wireless and batteryless 10-bit implantable blood pressure sensing microsystem with adaptive RF powering for real-time laboratory mice monitoring," *IEEE Journal of Solid-State Circuits*, 2009, vol. 44, no. 12, pp. 3631-3644.

[4] H. Cao, S. K. Thakar, T. Fu, M.Sheth, M. L. Oseng, V. Landge, Y.-S. Seo, J.-C. Chiao, "A Wireless Strain Sensor System for Bladder Volume Monitoring,"*In Proceedings of the IEEE MTTS International Microwave Symposium Digest (MTT)*, Baltimore, MD, USA, 5–10 June 2011; pp. 1–4.

[5] R. Jegadeesan, Y.-X. Guo, J.Minkyu, "Electric near-field coupling for wireless power transfer in biomedical applications," *in Proc. IEEE MTTS Int. Microw. Workshop Ser. RF Wireless Technol. Biomed. Healthcare Appl*., 2013, pp. 1–3.

[6] Vandevoorde G., Puers R, "Wireless Energy Transfer for Stand-alone Systems: a Comparison Between Low and High Power Applicability," *Sensor and Actuators a Physical*, 2001, vol. 92, No 1–3, pp. 305–311.

[7] A. K. RamRakhyani, and G. Lazzi, "Multicoil Telemetry System for Compensation of Coil Misalignment Effects in Implantable Systems," *IEEE Antennas and Wireless Propagation Letters*, 2012, vol. 11, pp. 1675-1678.

[8] D. Ahn and S. Hong, "Effect of Coupling Between Multiple Transmitters or Multiple Receivers on Wireless Power Transfer," *IEEE Transactions on Industrial Electronics*, 2013, vol. 60, no. 7, pp. 2602-2613.

[9] A. K. RamRakhyani, S. Mirabbasi, and C. Mu, "Design and Optimization of Resonance-Based Efficient Wireless Power Delivery Systems for Biomedical Implants," *IEEE Transactions on Biomedical Circuits and Systems*, 2011, vol. 5, no. 1, pp. 48-63.

[10] G. Yilmaz and C. Dehollaini, "An Efficient Wireless Power Link for Implanted Biomedical Devices via Resonant Inductive Coupling*," in Proc. of IEEE Radio and Wireless Symposium (RWS)*, 2012.

[11] X. Li, H. Zhang, F. Peng, Y. Li, T. Yang, B. Wang, et al., "A wireless magnetic resonance energy transfer system for micro implantable medical sensors," *Sensor*, 2012, vol. 12, no. 8, pp. 10292–10308.

[12] D.-W. Seo, J.-H. Lee, H. Lee, "Study on two-coil and four-coil wireless power transfer systems using z-parameter approach", *ETRI J*., 2016, vol. 38, no. 3, pp. 568-578.

[13] S. Atluri, M. Ghovanloo, "Design of a wideband power-efficient inductive wireless link for implantable biomedical devices using multiple carriers", *Proc. IEEE EMBS Conf. Neural Eng*.,2005, pp. 533-537.

[14] Jow U.-M. and Ghovanloo M., "Design and Optimization of Printed Spiral Coils for Efficient Transcutaneous Inductive Power Transmission," *IEEE Transactions on Biomedical Circuits and Systems*, 2007, vol. 1, pp. 193-202.

[15] Baker, M.W.; Sarpeshkar, R., "Feedback Analysis and Design of RF Power Links for Low-Power Bionic Systems," *IEEE Transactions on Biomedical Circuits and Systems*, 2007, vol.1, no.1, pp.28-38.

[16] J. Coulombe, M. Sawan, and J.-F. Gervais, "A highly flexible system for microstimulation of the visual cortex: Design and implementation," *IEEE Trans. Biomed. Circuits Syst*., Dec. 2007, vol. 1, no. 4, pp. 258–69.

[17] Artan, N; Vanjani, Hitesh; Vashist, Gurudath; Fu, Zhen; Bhakthavatsala, Santosh; Ludvig, Nandor; Medveczky, Geza; Chao, H, "A high-performance transcutaneous battery charger for medical implants," *2010 Conference Proceedings (IEEE Engineering in Medicine & Biology Society)*, 2010, vol. 1, pp. 1581-1584.

[18] S. Aldhaher, P. C.-K. Luk, and J. F. Whidborne, "Electronic tuning of misaligned coils in wireless power transfer systems," *IEEE Trans. Power Electron*., 2014, vol. 29, no. 11, pp. 5975–5982.

[19] N. de N. Donaldson, and T. A. Perkins, "Analysis of resonant coupled coils in the design of radio-frequency transcutaneous links," *Med. Biol. Eng. Comput*., 1983, vol. 21, pp. 612-627.

[20] D. C. Galbraith, M. Soma, and R. L. White, "A wide-band efficient inductive transdermal power and data link with coupling insensitive gain," *IEEE Trans. Biomed. Eng.*, Apr. 1987, vol. BME-34, pp. 265-275.

[21] M. Kiani and M. Ghovanloo, "An RFID-based closed-loop wireless power transmission system for biomedical applications," *IEEE Trans. Circuits Syst. II: Exp. Briefs*, Apr. 2010, vol. 57, no. 4, pp. 260–264.

[22] M. Fu, T. Zhang, X. Zhu, C. Ma, "A 13.56 MHz wireless power transfer system without impedance matching networks", 2013,*Proc.WPTC2013*, pp. 222-225.

[23] V. Valente, C. Eder, A. Demosthenous, and N. Donaldson, "Towards a closed-loop transmitter system with integrated class-D amplifier for coupling-insensitive powering of implants," in Proc. IEEE 19th Int. Conf. Electron. Circuits Syst., Dec. 2012, pp. 29–3.

[24] M. Ghovanloo, K. Najafi, "A wideband frequency-shift keying wireless link for inductively powered biomedical implants", *IEEE Transactions on Circuits and Systems*, Dec. 2004vol. 51, no. 12, pp. 2374-2383.

[25] C. Sauer, M. Stanac´evic´, G. Cauwenberghs, and N. Thakor, "Power harvesting and telemetry in CMOS for implanted devices," *IEEE Trans. Circuits Syst. I, Reg. Papers*, 2005, vol. 52, no. 12, pp. 2605–2613.

[26] T. Lehmann and Y. Moghe, "On-chip active power rectifiers for biomedical applications*," in Proc. IEEE Int. Symp. Circuits and Systems (ISCAS)*, May 2005, pp. 732–735.

[27] Y. H. Lam, W. H. Ki, and C. Y. Tsui, "Integrated low-loss CMOS active rectifier for wirelessly powered devices," *IEEE Trans. Circuits Syst. II, Expr. Briefs*, 2006, vol. 53, no. 12, pp. 1378–1382.

[28] S. Guo, and H. Lee, "An efficiency-enhanced CMOS rectifier with unbalanced-biased comparators for transcutaneous-powered high-current implants," *IEEE J. Solid State Circuits,* 2009, vol. 44, no. 6, pp. 1796 – 1804.

[29] H.-M. Lee and M. Ghovanloo, "An integrated power-efficient active rectifier with offset-controlled high speed comparators for inductively powered applications," *IEEE Trans. Circuits Syst. I, Reg. Papers*, 2011, vol. 58, no. 8, pp. 1749–1760.

[30] F. Zhang, S. A. Hackworth, X. Liu, H. Chen, R. J. Sclabassi and M. Sun, "Wireless Energy Transfer Platform for Medical Sensors and Implantable Devices," *in Proc. of International Conference of the IEEE Engineering in Medicine and Biology Society*, 2009, pp. 1045-1048.

[31] M. Bartoli, N.Noferi, A.Reatti, M.Kazimierczuk, "Modeling Litz-wire winding losses in high-frequency power inductors,"*Journal of Circuits, Systems and Computers*, 1996. vol. 5, pp. 1690-1696.

[32] R. F. Xue, K.-W. Cheng, and M. Je, "High-Efficiency Wireless Power Transfer for Biomedical Implants by Optimal Resonant Load Transformation," *IEEE Transactions on Circuits and Systems I: Regular Papers*, 2013, vol. 60, no. 4, pp. 867-874.

[33] Li, X., Li, Y., Guo, W. et al., "Wireless magnetic resonant energy transfer system based on micro 3D flexible MEMS Litz coils," *MicrosystTechnol*, 2014, vol. 20, p. 477.

[34] Hämmerle F., "Simulation and Characterization of a Miniaturized Planar Coil," Master thesis, 2009.

[35] A. Qusba, A. K. RamRakhyani, J. So, G. J. Hayes, M. D. Dickey, and G. Lazzi, "On the Design of Microfluidic Implant Coil for Flexible

Telemetry System," *IEEE Sensors Journal*, 2014, vol. 14, no. 4, pp. 1074-1080.
[36] Helwig B. G., Blaha M. D. and Leon L. R., "Effect of Intraperitoneal Radiotelemetry Instrumentation on Voluntary Wheel Running and Surgical Recovery in Mice," *Journal of the American Association for Laboratory Animal Science*, 2012 Sep; 51(5): 600–608.
[37] J. C. Maxwell, *A Treatise on Electricity and Magnetism*, Oxford Clarendon Press, 1873.
[38] F. W. Grover, *Inductance Calculations*, New York: Van Nostrand, 1946.